Thin Solid Films 518 (2010) 7291–7294

Contents lists available at ScienceDirect

Thin Solid Films

journal homepage: www.elsevier.com/locate/tsf

Carrier dynamics in InGaN/GaN multiple quantum wells based on different polishing processes of sapphire substrate

Hsiang-Chen Wang [a,*], Shih-Wei Feng [b], T. Malinauskas [c], K. Jarasiunas [c], Chu-Chi Ting [a], Sean Liu [d], Chin-Yi Tsai [b]

[a] Graduate Institute of Opto-Mechatronics, National Chung Cheng University, Chia-Yi, 62102, Taiwan, ROC
[b] Department of Applied Physics, National University of Kaohsiung, Kaohsiung 81148, Taiwan, ROC
[c] Institute of Applied Research, Vilnius University, LT-10222 Vilnius, Lithuania
[d] Department of Electronic Engineering, National Formosa University, Yunlin 632, Taiwan, ROC

ARTICLE INFO

Available online 9 May 2010

Keywords:
Pattern sapphire substrate
Four-wave mixing
Green InGaN LEDs

ABSTRACT

We report on carrier dynamics in the green InGaN/GaN light emitting diodes grown by metal organic chemical vapor deposition. Two LEDs with the same structures grown on pattern sapphire substrates with different surface roughnesses were prepared for comparisons (samples A and B). Sample A had the smoother sapphire surface than sample B. Time-resolved four-wave mixing has been performed at room temperature using 351 and 420 nm picosecond pulses for excitation. The determined diffusion coefficient in the upper InGaN QWs of sample B was twice smaller than that in sample A. The latter observation of better carrier confinement in sample B correlated with higher light emission efficiency in it.

1. Introduction

InGaN light emitting diodes (LEDs) attract much attention due to the advantages of high efficiency, compact size, and energy saving. Spontaneous and piezoelectric polarization fields in InGaN multi quantum well (MQW) active regions lead to the quantum confined stark effect (QCSE) and the separation of the electron and hole wave functions in the quantum well. Hence, the emission efficiency is reduced and the emission wavelength is red-shifted. These problems become more severe for higher-indium InGaN devices [1]. However, as the indium (In) mole fraction increases, the QCSE and phase separation were enhanced, deteriorating the crystalline quality and optical properties of the InGaN alloys. In addition, In clusters tend to aggregate around the existing extended defects such as threading dislocations (TDs), promoting the formation of V-shape defects. Due to the poor structural quality of high-In content InGaN alloys, the performance of the state-of-the-art green LEDs is significantly lower than those of other commercial LEDs. The "green" gap, one of the bottlenecks for further progress in solid-state lighting, must be solved to develop efficient color-mixing white LEDs [2,3].

The lattice mismatch between InGaN layers and substrates is also an issue to optimize the emission efficiency of green LEDs. Epitaxial lateral overgrowth (ELOG) and Pendeo epitaxy were used to minimize the lattice mismatch between GaN and sapphire substrates and to reduce the defect density in InGaN layers [4]. The latter way is too complicated to be processed. One-step GaN growth on the maskless patterned sapphire substrates (PSSs) is a simplified method to increase the emission efficiency. High-efficiency LEDs can be fabricated on dislocation-free InGaN/GaN multiple quantum well (MQW) nanorod arrays by using a metal organic chemical vapor deposition (MOCVD) system [5]. Horng et al. fabricated conventional and patterned sapphire substrates (PSSs) by metal organic vapor phase epitaxy (MOVPE). It is evident that the improvement of the output power depends on both the defect reduction of ELOG GaN and the scattering of emitted light at the GaN/sapphire interface [6]. In addition, Gap et al. demonstrated nano-patterned sapphire substrates (NPSSs) fabricated by a chemical wet etching technology with nano-sized SiO_2 as masks. This is a simple and effective technology to reduce dislocation density and to improve the performance of GaN-based LEDs [7]. There were several studies devoted to growth of blue InGaN LEDs on PSSs. However, for green InGaN LEDs grown on PSSs, this method is less developed and the mechanisms for improving the emission efficiency are unknown.

The nonlinear four-wave mixing (FWM) technique is becoming a versatile tool for characterization of bulk crystals as well as semiconductor micro- and nano-structures, as it allows fast and reliable evaluation of novel optoelectronic materials and related technologies. The technique opens possibility to measure a number of

* Corresponding author.
E-mail address: hcwang@ccu.edu.tw (H.-C. Wang).

0040-6090/$ – see front matter.
doi:10.1016/j.tsf.2010.04.093

electrical parameters of semiconductors in an "all-optical" way, using well-established correlations between electrical and optical processes. The unique advantage of this technique is a possibility of direct analysis of carrier transport by varying a spacing of light interference pattern. The previous studies of InGaN materials by FWM technique were carried out in heterostructures and single quantum well samples [8–10]. Okamoto et al. demonstrated that the main reason of the reduction of η_{ext} for a large amount of In is not the increment of nonradiative recombination center, but the delocalization of carriers due to fast diffusion [8]. We presented that decay times of free carrier gratings with various spatial periods allowed determination of bipolar diffusion coefficient $D=2.1$ cm^2/s, effective carrier lifetime of 470 ps, and estimate the corresponding hole mobility 40 cm^2/V s at carrier density of about 10^{18} cm^{-3} [9]. To get deeper insight into correlation of photoelectric, transport, and structural properties of InGaN alloys, the nonequilibrium carrier dynamics and competition of nonradiative and radiative recombination in differently doped $In_xGa_{1-x}N$ heterostructures have been studied by TR FWM and PL techniques [10].

In this study, we present the optical analysis of green emission from InGaN MQW LEDs, grown on sapphire with different surface roughnesses. The grown structures were evaluated by using time-integrated luminescence and time-resolved four-wave mixing techniques. In Section 2, growth conditions and experimental procedures are discussed. The AFM images of the sapphire substrate, photoluminescence, and four-wave mixing results are presented in Section 3. Finally, the conclusions are drawn in Section 4.

2. Sample structures and experimental procedures

Two LED samples (samples A and B) with the same structures were grown on two kinds of *c*-plane PSSs by MOCVD. PSSs with different surface terrace patterns were prepared. As shown in Fig. 1, the layer structures of the LED samples consist of a 2 μm GaN buffer layer, a 2.5 μm *n*-GaN layer, a 30 nm $In_{0.01}Ga_{0.99}N$, three InGaN/GaN QW active regions with various In contents, and a 130 nm *p*-GaN cap layer. The bottom, middle, and upper active layer structures are four periods $In_{0.05}Ga_{0.95}N$/GaN, four periods $In_{0.06}Ga_{0.94}N$/GaN, and six periods $In_{0.2}Ga_{0.8}N$/GaN MQWs, respectively. The thicknesses of the well and barrier were about 2 and 7 nm, respectively.

PL measurements were carried out with the 325 nm line of a 50 mW He–Cd laser for excitation. Carrier dynamics in InGaN quantum wells and *p*-type GaN layer were investigated using picosecond four-wave mixing (FWM) technique [11]. A FWM scheme with diffraction optical element as a beam splitter and Nd: YLF laser as excitation source at 351 nm was used to record the transient free carrier grating [12]. The carriers were generated in a submicron-thick surface layer and their dynamics were monitored by the delayed probe beam at 1064 nm wavelength.

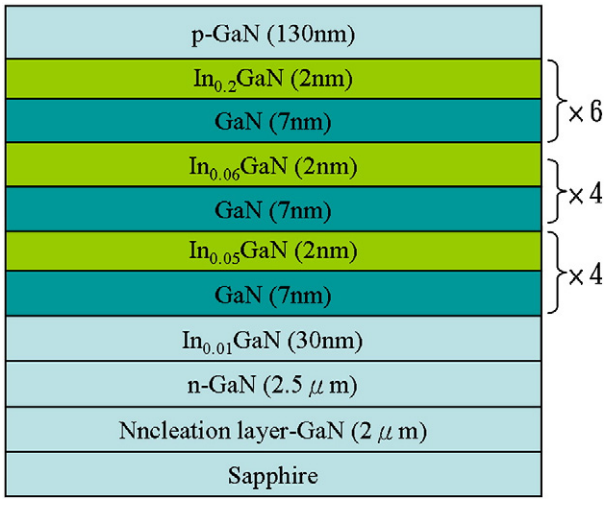

Fig. 1. Schematic picture of the multiple quantum well structure used in this work.

3. Results and discussions

3.1. AFM images of the sapphire substrates

The surface roughness of the PSSs was monitored with atomic force microscopy (AFM) measurement. The AFM images (0.8×0.8 μm^2) of samples A and B were shown in Fig. 2(a) and (b). Fig. 2(c) and (d) shows the line-scan profiles in an atomic force microscopy (AFM) measurement of samples A and B, respectively. One can see the terrace of sample A with the scales of 32.8 nm in width and 0.1 nm in height (0.063 nm in rms roughness). Sample B with different polishing processes has a dimension of the terrace of about 60.9 nm in width and 0.25 nm in height (0.12 nm in rms roughness). Here we can see that the substrate of sample A has the smoother surface than sample B.

3.2. Photoluminescence

Fig. 3 shows the temperature-dependent PL peak energy and integrated intensity. In each sample, the temperature-dependent PL peak energy exhibited an S-shape behavior. The S-shape behavior has been attributed to the carrier dynamics associated with carrier localization in potential minimums [13,14]. The relatively higher PL intensity of sample B at high temperatures suggests that the internal quantum efficiency of sample B is higher than that of sample A. The PL peak position of sample B shows a blue shift to that of sample A. This implies that a highly rough surface substrate can release more strain in InGaN MQW layers. In such condition, the weaker Quantum Confined Stark Effect (QCSE) in sample B leads to the blue shift of emission wavelength [15].

3.3. Four-wave mixing

The picosecond nondegenerate FWM technique has been demonstrated in Reference [12]. The energy of the grating recording beam (I_0), intensities of the transmitted (I_T), diffracted probe beam (I_D), and background signal (I_B) (the scattered light intensity in the first diffraction) were recorded in the FWM measurement. The instantaneous diffraction efficiency $\eta=(I_D-I_B)/I_T$ and its kinetics $\eta(t)\propto[\Delta N_{t=0}\exp(-t/\tau_G)]^2$ were measured at different grating periods and used for determination of the carrier lifetime τ_R and the diffusion coefficient D. The excitation energy density range I_0 (=0.5–8 mJ/cm^2) corresponds to excess carrier density above $5\cdot10^{18}$ cm^{-3}. If the absorption coefficient at 351 nm is $7\cdot10^4$ cm^{-1}, this carrier density corresponds only to the surface of the photoexcited layer. Carrier recombination and diffusion diminished the high plasma density in the cap layer (it is known that very fast carrier recombination rate is typical for Mg-doped GaN [9]). The incident light also penetrated to the InGaN/GaN MQWs below the cap layer and created free carriers. In addition, the carriers were rapidly transferred from the cap layer and the GaN barriers to the InGaN wells. Therefore, we assumed that the subsequent grating decay after the end of the laser pulse was determined mainly by the processes in the upper InGaN active region. Kinetics of the diffraction efficiency at 351 nm excitation were shown in Fig. 4(a) and (b) for sample A/B. For comparison, we also realized direct carrier injection to the quantum wells by using 420 nm picosecond pulses from the parametric oscillator. In the latter case, the light penetrated via the GaN cap without absorption losses and generated carriers only in the upper $In_{0.2}Ga_{0.8}N$ active layers. In the latter case, we observed much weaker diffraction and faster decay

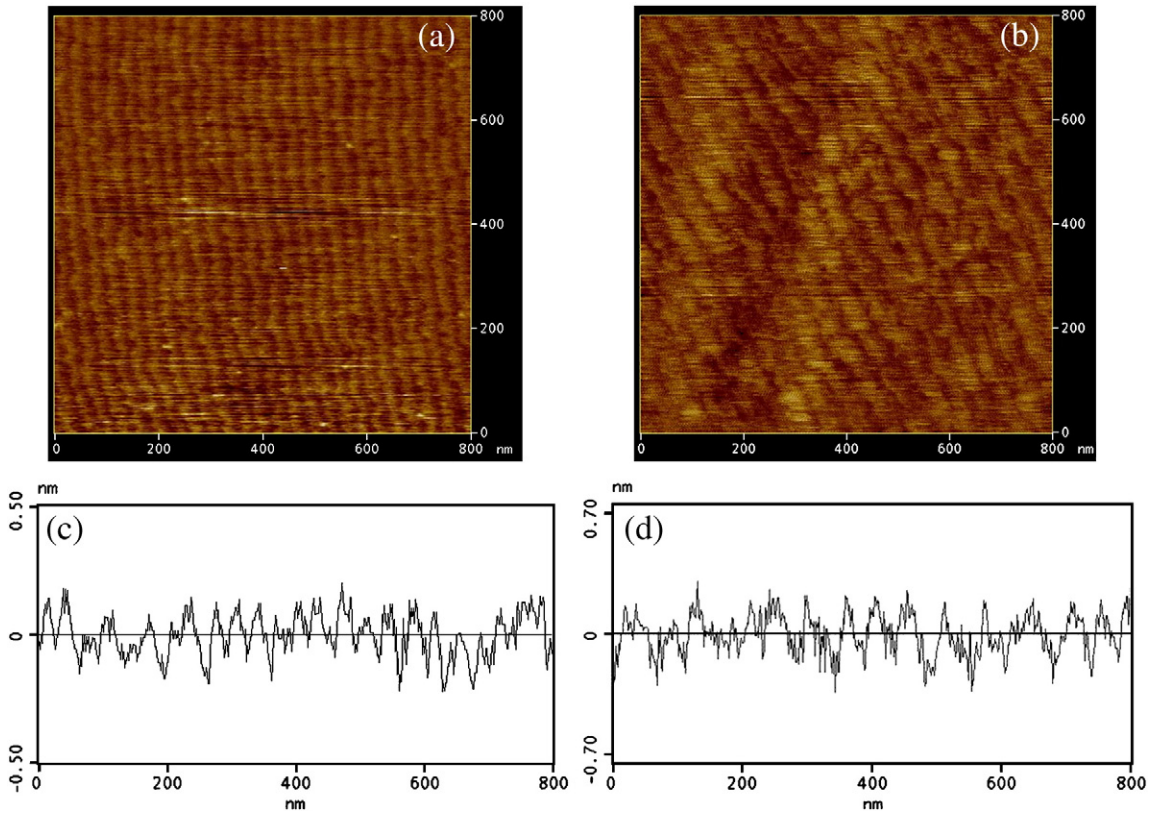

Fig. 2. AFM images of $0.8 \times 0.8\ \mu m^2$ in size of the substrate of sample A (a) and sample B (b); (c) an AFM line-scan profile of sample A; (d) an AFM line-scan profile of sample B.

signals, both in samples A and B. Therefore, further measurements for determination of diffusion coefficient and carrier lifetime were performed with 351 nm excitation.

In Fig. 5, we present the inverse grating decay time for different grating periods, and this dependence provided directly both D and τ_R values in the samples:

$$\frac{1}{\tau_G} = \frac{1}{\tau_R} + \frac{1}{\tau_D}, \quad \tau_D = \frac{\Lambda^2}{4\pi^2 D} \tag{1}$$

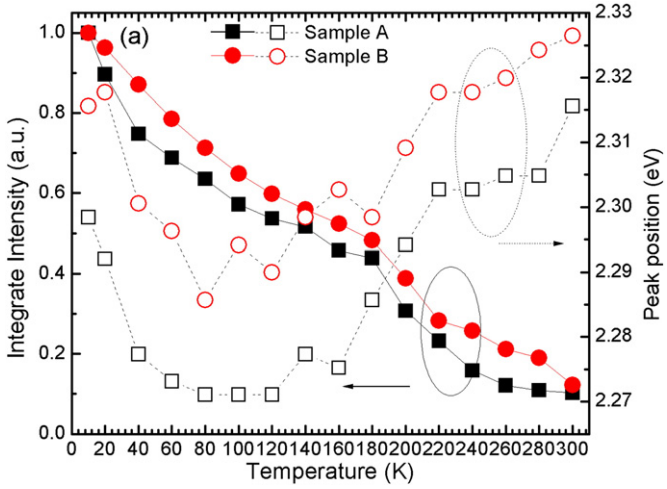

Fig. 3. Temperature dependence of integrated PL intensity and PL peak position for samples A and B. We note higher emission efficiency and longer emission wavelength for sample B.

where τ_R is the recombination time and τ_D is the diffusion time of the grating erasure. A slope of the plot provides D value, while the intersection with the ordinate axis provides the $1/\tau_R$ value. It was observed that $D = 0.9\ cm^2/s$ and $\tau_R = 1.2$ ns for sample B were smaller than those of sample A ($D = 2\ cm^2/s$ and $\tau_R = 1.7$ ns). Due to carrier localization effect, carrier diffusion coefficient of $In_{0.1}Ga_{0.9}N$ active layers also revealed a smaller D value down to $\sim 1\ cm^2/s$ [9]. For the $In_{0.2}Ga_{0.8}N$ active layers in this work, the localization effect is stronger (as evidenced by D value decrease). Due to a higher defect density in the higher-In InGaN layer, nonradiative recombination is enhanced and lifetime becomes shorter. Consequently, smaller amount of carriers would be localized and the average carrier lifetime became shorter. This situation was observed in carrier dynamics of $In_{0.15}Ga_{0.85}N$ [9]. On the other hand, localization may lead to a lower threshold of stimulated recombination and shorter photoluminescence decay times [10]. Therefore, the smaller D and τ_R values of sample B suggest a higher structural quality with respect to that of sample A. This observation is in agreement with a higher luminescence efficiency of sample B.

4. Conclusion

In summary, we investigated the optical properties of two green InGaN LEDs grown on sapphire with different roughness substrates. Photoluminescence data revealed higher emission efficiency and short emission wavelength in sample B with large dimension terraces on sapphire surface, which provided better strain release and stronger carrier localization effect in the QW structure. FWM measurements allowed determination of carrier diffusion coefficient and lifetime for the samples at carrier injection directly to the top QW structure with 20% of In. The determined diffusion coefficient was twice smaller in

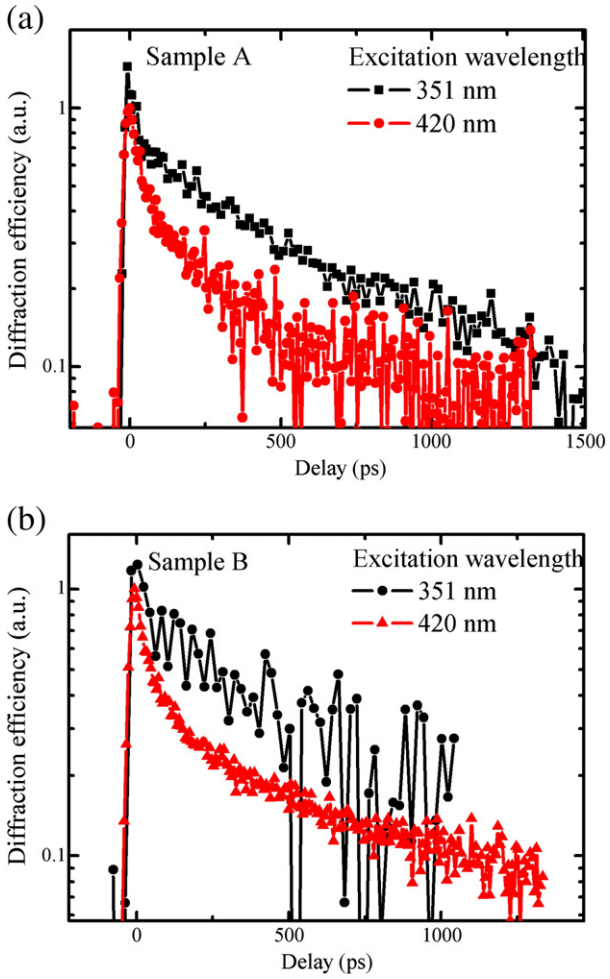

Fig. 4. Comparison of FWM signal decay at carrier injection directly to the QWs (excitation at 420 nm) or via the cap layer (excitation at 351 nm): (a) for sample A; (b) for sample B.

sample B, thus indicating better carrier confinement in the QWs. The latter observation correlated with higher light emission efficiency from sample B.

Acknowledgements

This research was supported by the National Science Council, The Republic of China, under Grant No. NSC 97-2221-E-194-008 and European Commission Contract No. MRTN-CT-2006-035735.

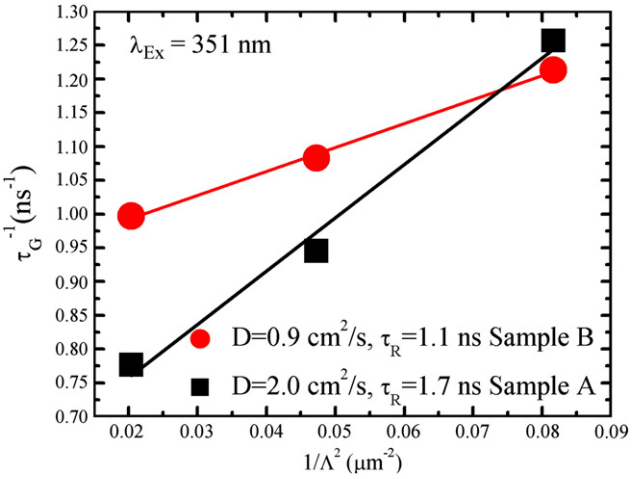

Fig. 5. Determination of diffusion coefficient and carrier lifetime in QWs at carrier injection from the cap layer.

References

[1] H. Zhao, G. Liu, X.-H. Li, G.S. Huang, J.D. Poplawsky, S.T. Penn, V. Dierolf, N. Tansu, Appl. Phys. Lett. 95 (2009) 061104.
[2] C. Bayram, F.H. Teherani, D.J. Rogers, M. Razeghi, Appl. Phys. Lett. 93 (2008) 081111.
[3] Y. Yang, X.A. Cao, C.H. Yan, Appl. Phys. Lett. 94 (2009) 041117.
[4] T.S. Ko, S.C. Ling, T.C. Lu, H.C. Kuo, S.C. Wang, Appl. Phys Lett. 91 (2007) 021914.
[5] H.M. Kim, Y.H. Cho, H. Lee, S.I. Kim, S.R. Ryu, D.Y. Kim, T.W. Kang, K.S. Chung, Nano Lett. 4 (2004) 1059.
[6] R.H. Horng, W.K. Wang, S.C. Huang, S.Y. Huang, S.H. Lin, C.F. Lin, D.S. Wuub, J. Cryst. Growth 298 (2007) 219.
[7] H. Gao, F. Yan, Y. Zhang, J. Li, Y. Zeng, G. Wang, J. Phys. D 41 (2008) 115106.
[8] K. Okamoto, A. Kaneta, K. Inoue, Y. Kawakami, M. Terazima, G. Shinomiya, T. Mukai, Sg. Fujita, Phys. Status Solidi B 228 (2001) 81.
[9] R. Aleksiejunas, M. Sudžius, V. Gudelis, T. Malinauskas, K. Jarašiunas, Q. Fareed, R. Gaska, M.S. Shur, J. Zhang, J. Yang, E. Kuokštis, M.A. Khan, Phys. Status Solidi C 7 (2003) 2686.
[10] K. Jarasiunas, R. Aleksiejunas, T. Malinauskas, S. Miasojedovas, S. Jursenas, A. Zukauskas, R. Gaska, J. Zhang, M.S. Shur, J.W. Yang, E. Kuokstis, M.A. Khan, Phys. Status Solidi A 202 (2005) 820.
[11] T. Malinauskas, R. Aleksiejunas, K. Jarašiunas, B. Beaumont, P. Gibart, A. Kakanakova-Georgieva, E. Janzen, D. Gogova, B. Monemar, M. Heuken, J. Cryst. Growth 300 (2007) 223.
[12] K. Jarasiunas, R. Aleksiejunas, T. Malinauskas, V. Gudelis, T. Tamulevicius, S. Tamulevicius, A. Guobiene, A. Usikov, V. Dmitriev, H.J. Gerritsen, Rev. Sci. Inst. 78 (2007) 033901.
[13] Y.H. Cho, G.H. Gainer, A.J. Fischer, J.J. Song, S. Keller, U.K. Mishra, S.P. DenBarrs, Appl. Phys. Lett. 73 (1998) 1370.
[14] P.G. Eliseev, P. Perlin, J. Lee, M. Osinski, Appl. Phys. Lett. 71 (1997) 569.
[15] Chih-Chung Teng, Hsiang-Chen Wang, Tsung-Yi Tang, Yen-Cheng Lu, Yung-Chen Cheng, C.C. Yang, Kung-Jen Ma, Wei-Ming Wang, Chi-Wei Hsu, L.C. Chen, J. Cryst. Growth 288 (2006) 18.